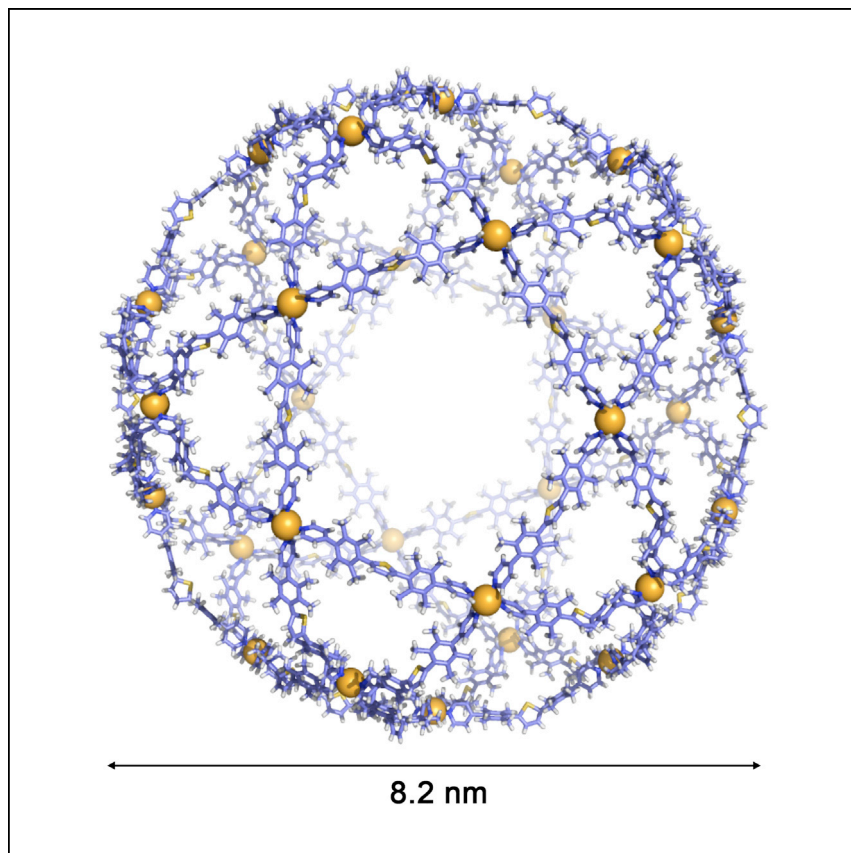


Article

Self-Assembly of $M_{30}L_{60}$ Icosidodecahedron

Bottom-up construction of giant structures by the self-assembly of a large number of components ($n = \sim 100$) has been a daunting challenge. Here, Fujita and colleagues report the self-assembly of a spherical metal polyhedron, possessing a hitherto unreported icosidodecahedron geometry with 30 vertices and 60 edges. The authors succeeded in controlling the self-assembly by intensive tuning of the ligand flexibility. X-ray crystallographic analysis confirmed that the complex is the largest well-defined spherical molecular capsule, comparable with the size of a typical protein.

Daishi Fujita, Yoshihiro Ueda,
Sota Sato, Hiroyuki Yokoyama,
Nobuhiro Mizuno, Takashi
Kumasaka, Makoto Fujita

mfujita@appchem.t.u-tokyo.ac.jp

HIGHLIGHTS

Self-assembly of an $M_{30}L_{60}$
icosidodecahedron

Bridging ligand design for
flexibility tuning

Crystallization and fine X-ray
analysis of $M_{30}L_{60}$

ACCESSION NUMBERS

CCDC: 1482268

Article

Self-Assembly of $M_{30}L_{60}$ Icosidodecahedron

Daishi Fujita,^{1,2,5} Yoshihiro Ueda,^{1,5} Sota Sato,³ Hiroyuki Yokoyama,¹ Nobuhiro Mizuno,⁴ Takashi Kumasaka,⁴ and Makoto Fujita^{1,6,*}

SUMMARY

Self-assembly is invaluable in the construction of giant molecular structures via a bottom-up approach. Although living organisms naturally make the most use of self-assembly and freely handle the mechanism at will, scientists are still far behind the level of nature. Inspired by the elegant structures of virus capsids, we have previously constructed roughly spherical giant metal complexes with the symmetry of an octahedron, cuboctahedron, and rhombicuboctahedron with the compositions M_6L_{12} , $M_{12}L_{24}$, and $M_{24}L_{48}$, respectively. Here, we report our first successful synthesis of an $M_{30}L_{60}$ molecular icosidodecahedron that consists of ~ 100 components: 30 Pd(II) ions and 60 ligands that assemble into the largest well-defined spherical macromolecule to date (diameter of ~ 8.2 nm). Tuning the flexibility of the ligand was the key for successful self-assembly. A highly complex but symmetrically organized structure was identified through X-ray crystallographic analysis. The interior space of the molecular complex is large enough ($157,000 \text{ \AA}^3$) to enclose proteins.

INTRODUCTION

Molecular self-assembly commonly underlies the creation of various biological macromolecules. It enables the construction of giant structures of a size not practically attainable by a single molecular unit. Ferritin¹, COPII coat cage,^{2,3} and various virus capsids^{4,5} are representatives from nature's many examples. Inspired by this elegant biology, scientists have long pursued a way to emulate and acquire equally impressive molecular self-assembly constructs and strategies.^{6–14} The design of molecular self-assembly constructs with fewer than ten components, or at most a couple of dozen, has become routine;^{15–27} however, self-assembly from a number of components comparable with that seen in nature (~ 100 components) is still inherently challenging. Part of this challenge lies in the fact that the process of self-assembly and the final structure obtained strongly depend on the number and precise nature of the initial components. For example, when trying to predict the final self-assembled structure of a newly synthesized ligand using results obtained from another, almost identical ligand possessing a structure with only subtle differences, these tiny differences become amplified during self-assembly, making the structure of the final product difficult to forecast. As a result, rational design strategies and mechanistic discussion regarding molecular self-assembly for synthetic macromolecules are extremely important but still unexplored.

We have been tackling this uncharted area by utilizing self-assembly of divalent Pd^{2+} ions (M) and ditopic pyridyl ligands with a bend angle (L), which gives giant spherical metal complexes with the composition M_nL_{2n} .²⁸ They are regarded as the largest class of molecules with unambiguous structures that have ever been synthesized. The topology of M_nL_{2n} self-assembled cages can be described as polyhedra, where the Pd^{2+} ions are regarded as vertices and the ligand as edges. Because Pd^{2+} has

The Bigger Picture

The technology we report here is a milestone for the development of nanotechnology. There are two opposite approaches to fabricating accurate nanometer-sized structures: top-down and bottom-up approaches. The top-down approach, typically using photolithography techniques, has developed rapidly along with the semiconductor industry and has reached the level whereby they can handle single-digit nanometers. However, this approach is already getting close to the theoretical limit with no further room for development; control of the structure with atomic-level accuracy, at least, will not be possible. In this respect, the bottom-up approach is highly promising for the manipulation of matter of interest with atomic-level accuracy, although this approach is still too premature for building structures bigger than multiple nanometers. Here, we have built a giant (8 nm) molecular architecture by self-assembling ~ 100 components. This report pushes our technological progress to the next level.

four coordination sites with square planar geometry, self-assembled M_nL_{2n} polyhedra are consequently limited to equilateral and tetravalent polyhedra. Isotropic (ideally spherical) structures are favored because of the minimization of surface energy, resulting in the formation of Platonic and Archimedean solids. Given these geometric constraints, only five such structures can be theoretically obtained and are illustrated in the road map (Figure 1A), namely M_nL_{2n} polyhedral with $n = 6, 12, 24, 30,$ and 60 . So far, we have succeeded in synthesizing the M_6L_{12} octahedron ($n = 6$),²⁹ $M_{12}L_{24}$ cuboctahedron ($n = 12$),³⁰ and $M_{24}L_{48}$ rhombicuboctahedron ($n = 24$).³¹

As the next logical step, we aimed to synthesize the $M_{30}L_{60}$ ($n = 30$) polyhedron. However, $M_{30}L_{60}$ was not a simple extension of the previous ones ($n \leq 24$) for the following reasons. First, the effect of kinetic trapping during the self-assembly process is no longer negligible. This effect was not a critical problem when $n = 6, 12,$ or 24 because intermediate, incomplete structures can still form and unform reversibly. As the number of components participating in the self-assembly increases, however, the formation of more meta-stable intermediates becomes possible, at least some of which are kinetically trapped products. We propose that this type of mechanism involving kinetically trapped intermediates is reminiscent of the folding funnel hypothesis for protein folding.³² Second, the symmetry group is different. Even though all of the previously synthesized polyhedra with $n = 6, 12,$ or 24 have cubic symmetry, polyhedra with $n = 30$ or 60 adopt dodecahedral symmetry that contains pentagon faces. As shown in Figure 1B, the pentagon results in two different and ill-balanced interior angles, 60° and 108° . Thus, rational ligand design to allow for this structural difference is the key to obtaining self-assembled structures with $n > 24$. In this study, we addressed the foregoing scientific hurdles with a finely designed flex-tuned ligand, which allowed us to obtain the $M_{30}L_{60}$ icosidodecahedral self-assembled metal complex, the structure of which was determined by single-crystal X-ray structural analysis. The polyhedron consists of precisely 90 subcomponents, the diameter of which reaches 8.2 nm, which is comparable in size with biological macromolecules such as proteins.

RESULTS AND DISCUSSION

Ligand Design and Self-Assembly

When designing M_nL_{2n} self-assembled systems, we have long focused on the ligand bend angles as a guiding principle.³³ In theory, the ideal bend angle θ can be calculated mathematically for any target polyhedral, for example, $\theta = \sim 90^\circ$ for M_6L_4 , $\theta = \sim 120^\circ$ for $M_{12}L_{24}$, and $\theta = \sim 135^\circ$ for $M_{24}L_{48}$. For $n \leq 24$,^{29,30,34} this guiding principle works well. However, we found that the self-assembly of thiophene-cored ligand (1, $\theta = 149^\circ$), even with a θ value close to the ideal bend angle for $M_{30}L_{60}$ ($\theta = 150^\circ$), still formed $M_{24}L_{48}$ rather than $M_{30}L_{60}$.³¹ This observation suggests that the effect of kinetic trapping becomes dominant at $n > 24$; the $M_{24}L_{48}$ complex 2 from ligand 1 is likely a kinetically trapped structure in an energy local minimum close to $M_{30}L_{60}$ on the self-assembly potential profile.³³

We thus sought a way to bring the trapped structure out of the local minimum. After 2 was prepared by mixing 1 and $\text{Pd}(\text{NO}_3)_2$ at 70°C for 1 hr in dimethylformamide (DMF) (Figure 2A), the DMF solution was further heated at 70°C for 12 hr. Mass spectrometry showed the formation of the $M_{30}L_{60}$ species with significant intensity in the spectrum (Figure 2B). This observation confirms the idea that the $M_{24}L_{48}$ complex 2 is the kinetic species prior to assembling into the thermodynamic product $M_{30}L_{60}$. Prolonged heating of the solution did not change the $M_{24}L_{48}/M_{30}L_{60}$ ratio.

¹Department of Applied Chemistry, Graduate School of Engineering, The University of Tokyo, 7-3-1 Hongo, Bunkyo-ku, Tokyo 113-0033, Japan

²PRESTO (Precursory Research for Embryonic Science and Technology), Japan Science and Technology Agency, 7-3-1 Hongo, Bunkyo-ku, Tokyo 113-0033, Japan

³Advanced Institute for Materials Research, Tohoku University, 2-1-1 Katahira, Aoba-ku, Sendai 980-8577, Japan

⁴Japan Synchrotron Radiation Research Institute (JASRI/SPRING-8), 1-1-1 Kouto, Sayo-cho, Sayo-gun, Hyogo 679-5198, Japan

⁵Co-first author

⁶Lead Contact

*Correspondence:
mfujita@appchem.t.u-tokyo.ac.jp

<http://dx.doi.org/10.1016/j.chempr.2016.06.007>

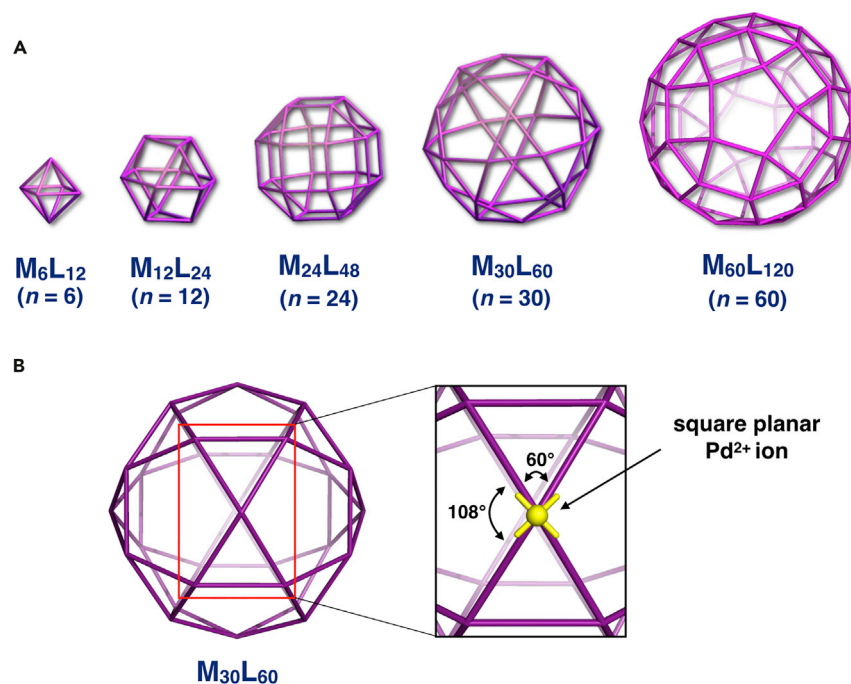


Figure 1. Schematic Representation of M_nL_{2n} Self-Assembly

(A) The family of M_nL_{2n} polyhedra. Metals (M) and bridging ligands (L) are mapped onto the vertices and edges of the polyhedral, respectively.

(B) An enlarged view around a vertex of the icosidodecahedron ($M_{30}L_{60}$). The two different interior angles, 60° and 108°, are ill balanced with respect to the Pd²⁺ square planar coordination geometry.

Instead, partial decomposition of the complexes was observed, and we were unable to isolate and characterize the $M_{30}L_{60}$ complex by other spectroscopic or crystallographic methods.

To suppress the formation of $M_{24}L_{48}$ and facilitate the self-assembly of $M_{30}L_{60}$, we reasoned that a strategy to accommodate pentagon faces into the assembly process is of significant importance. The designed ligand should have flexibility to avoid ill-balanced interior angles, but flexible ligands are more likely to be kinetically trapped in smaller structures with fewer components. In order to balance the two competing factors, we tuned the ligand flexibility by chemically varying the spacer moiety, i.e., the connector between the center thiophene and the side pyridyl groups.

Ligand **3a**, equipped with an ethynylene spacer group, was first examined. When this ligand was treated with 0.51 equivalent of $[Pd(MeCN)_4](BF_4)_2$ in DMSO-*d*₆ at 70°C for 2 hr, peak broadening and downfield shifts of the aromatic protons were observed in the ¹H nuclear magnetic resonance (NMR) spectrum (Figure S23), a commonly observed phenomenon in the formation of large structures.³¹ However, the diffusion coefficient values of self-assembled products, evaluated by ¹H diffusion ordered spectroscopy (DOSY) NMR experiments, suggested that the self-assembled products did not converge into a single species. Instead, the reaction gave a mixture of products with diffusion coefficients consistent with $M_{12}L_{24}$ or even smaller self-assembled products.³⁵ This observation implied that this ligand, being too flexible, favors the formation of kinetic products yielding smaller polyhedral structures by distorting the ligand frame to an arch shape.³⁶

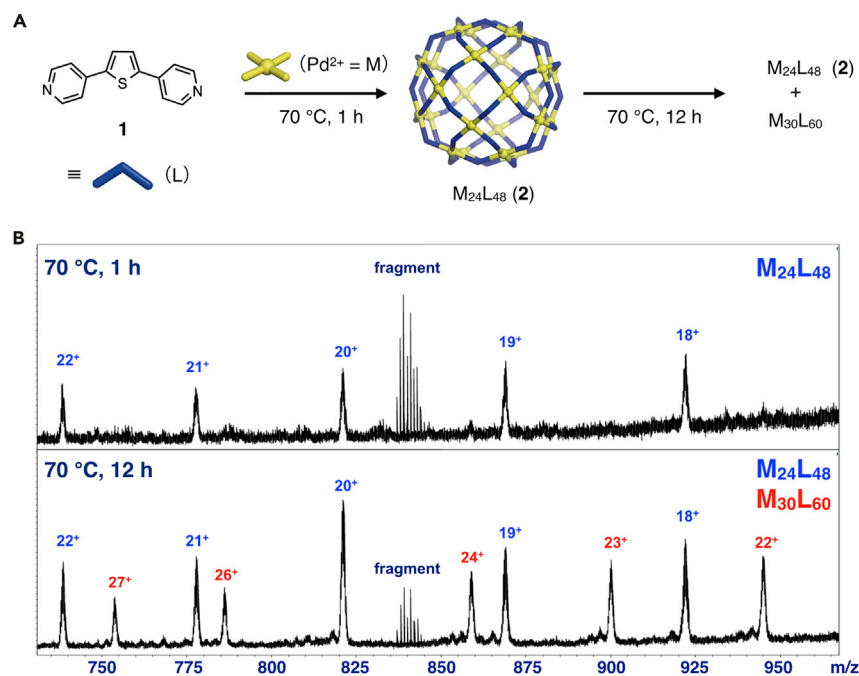


Figure 2. Self-Assembly of M_nL_{2n} Complexes from Thiophene-Cored Ligand 1 and Pd^{2+} Ion
Reaction scheme (A) and mass spectrometric data (B) after heating the components at $70\text{ }^\circ\text{C}$ for 1 hr (top) and subsequently for 12 hr (bottom) in DMF.

We next focused on more rigid phenylene-based spacers. Ligands 3b–3d, shown in Figure 3, were newly designed. Unfortunately, ligand 3b, with a simple phenylene spacer, was not suitable for experiments because of its low solubility. For ligands 3c and 3d, the introduction of methyl groups sterically disturbs the π -conjugation of the planar conformation and thus enhances their solubility in DMF. Whereas ligand 3c only affords a complex mixture (Figure S25), the tetramethylphenylene spacer 3d showed a promising NMR spectrum when heated with 0.51 equivalent of $\text{Pd}(\text{BF}_4)_2(\text{CH}_3\text{CN})_4$ in $\text{DMF-}d_7$ at $70\text{ }^\circ\text{C}$ for 12 hr (Figure 4). Three broad peaks were observed in the ^1H NMR spectrum in the range of 10–6 parts per million (ppm) (Figure 4C). The peaks at 9.8, 7.8, and 7.0 ppm were assigned to PyH_α , PyH_β , and thiophene proton, respectively. Downfield shifts of PyH_α ($\Delta\delta = 1.04$ ppm) and PyH_β ($\Delta\delta = 0.49$ ppm) indicated Pd^{2+} coordination, and the broad and simple signals were consistent with the formation of a very large structure with high symmetry. In this spectrum, all of the pyridine rings seemed to be equivalent, which suggested the formation of the $\text{M}_{12}\text{L}_{24}$ cuboctahedron or the $\text{M}_{30}\text{L}_{60}$ icosidodecahedron by symmetry considerations. ^1H DOSY NMR also indicated the formation of a single product with a diffusion coefficient (D) of $6.6 \times 10^{-11} \text{ m}^2 \text{ s}^{-1}$ ($\log D = -10.18$) at 300 K in $\text{DMF-}d_7$ (Figure 4D). The observed D value is much smaller than that of the corresponding $\text{M}_{12}\text{L}_{24}$ complex (see Supplemental Experimental Procedures), an observation that is also consistent with the construction of the first $\text{M}_{30}\text{L}_{60}$ complex 4.

The $\text{M}_{30}\text{L}_{60}$ composition was confirmed by cold-spray ionization time-of-flight mass spectrometry (CSI-TOF MS)³⁷ (Figure S9). A series of prominent peaks of $[\text{4}-(\text{BF}_4)_m + (\text{DMF})_n]$ (with m values from 20 to 30 and n values from 0 to 8) was observed, and no other peaks with significant intensity were detected. Although the resolution of the spectrum was not that high and we could not clearly distinguish their isotope

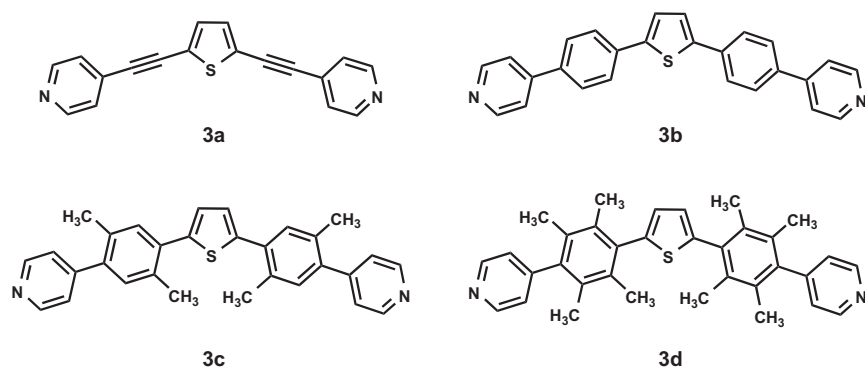


Figure 3. Newly Designed Flexible Ligands 3a–3d

distributions, it is rather surprising that such a giant $M_{30}L_{60}$ complex was stable enough to be detected by mass spectrometry at all.

X-Ray Crystallographic Analysis

The 3D coordination geometry of the $M_{30}L_{60}$ was clearly demonstrated by X-ray crystallographic analysis (Figure 5). After years of attempts, we found that a single crystal of **4** could be grown under extremely slow vapor diffusion (2–3 months) of $\text{AcO}i\text{Pr}$ into a DMSO solution of **4**. Although the crystals obtained were mechanically fragile and unstable upon solvent evaporation, we overcame this hurdle by improving our crystal-handling techniques (e.g., handling the crystals under refrigerated temperatures). Since crystals of **4** contained significantly larger volumes of solvent (revealed to be 90% of volume after analysis), small structured mosaics within the crystals tended to form upon freezing. Thus, we opted to collect data at room temperature, as it yielded better results with lower mosaicity than when collected at 100 K. In the end, we obtained high-quality data up to 2.0 Å resolution by synchrotron X-ray radiation (BL38B1 and BL41XU at SPring-8 and BL1A at KEK PF-AR). The diffraction data resembled those of protein crystals rather than conventional metal complexes. Large unit cell volume ($a = 122.3$ Å, $b = 78.3$ Å, $c = 78.8$ Å, and $\beta = 121.8^\circ$) and extremely large void space (90%) made the crystallographic data unique. The typical procedure of small-molecule X-ray analysis and statistical criteria no longer worked. Therefore, the model building was carried out through ligand/solvent model alignment on the $2F_o - F_c$ map and the maximum entropy method^{38,39} electron-density map in a manner analogous to protein crystallography. The refinement model of the spherical complex was calculated by the CGLS command in SHELX,⁴⁰ instead of LS, which is typically used for small molecules.

The X-ray structure shows a flawless icosidodecahedral geometry as designed (Figure 5). The cloudless electron-density map surely proves the existence and the connectivity of the icosidodecahedral structure (Figure 5A). Although bond lengths and angles do not perfectly conform to the abstract geometric mathematical structure, as might be expected, the overall topology of the structure is perfectly consistent. Because of its flexibility, the framework assembled by ligand **3d** is slightly sagged (Figure 5B) so that all $N_{\text{pyridine}}\text{-Pd(II)-}N_{\text{pyridine}}$ angles involved in triangle and pentagon faces are adjusted to be around 90° , an ideal angle for Pd(II) square planar geometry (Figure 5C). The diameter of the circumscribed sphere abstracted around the complex is 8.2 nm, and the inscribed sphere is 6.7 nm. It is notable that solvents occupy 90.0% of the total cell volume. As these solvents are not structured in the void, no distinguishable electron-density peak was observed, except the ones weakly coordinated to the aromatic rings of the ligands (Figure 5D). The

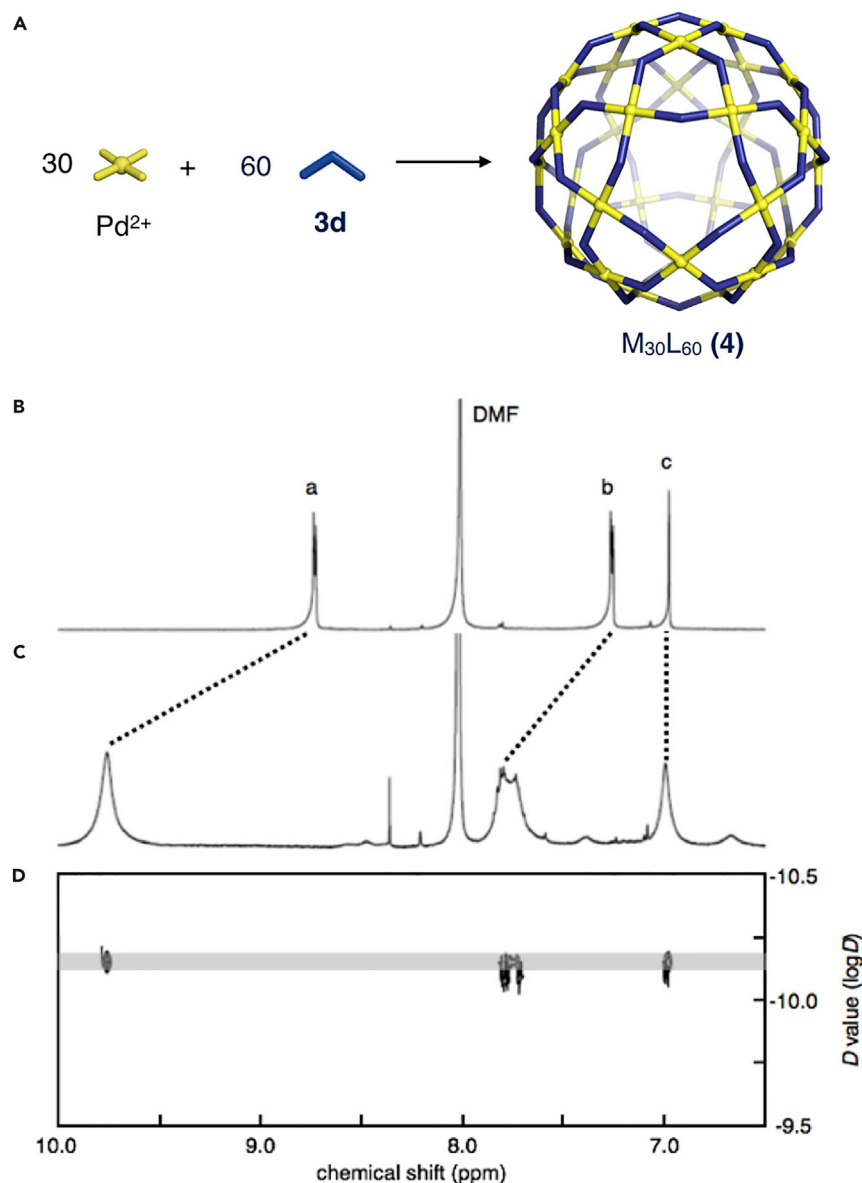


Figure 4. Self-Assembly of $\text{M}_{30}\text{L}_{60}$ Icosidodecahedron

(A) The reaction scheme. Ligand **3d** was treated with Pd^{2+} ion in a 2:1 ratio at 70°C for 12 hr in DMF-d_7 .
 (B) ^1H NMR spectrum of ligand **3d**. Signals a, b, and c denote PyH_{α} , PyH_{β} , and thiophene protons, respectively.
 (C) ^1H NMR spectrum of complex **4** (BF_4^- salt). Aromatic signals shifted to downfield and heavily broadened.
 (D) ^1H DOSY spectrum of sphere **4** (500 MHz, DMF-d_7 , 300 K). The spectrum indicates a single product with a diffusion coefficient (D) of $6.6 \times 10^{-11} \text{ m}^2 \text{ s}^{-1}$ ($\log D = -10.18$). All the NMR spectra (500 MHz) were measured as DMF-d_7 solution at 300 K.

coordination of DMSO to aromatic rings (lone-pair- π interactions) is a known phenomenon.⁴¹ Most of the atoms other than oxygen were severely disordered in this case. The sliced view of the spherical complex (Figure 5E) visually affirms the statements mentioned above and that our model building is sufficient. Even though there is no comparable example in the literature, considering such a huge void space

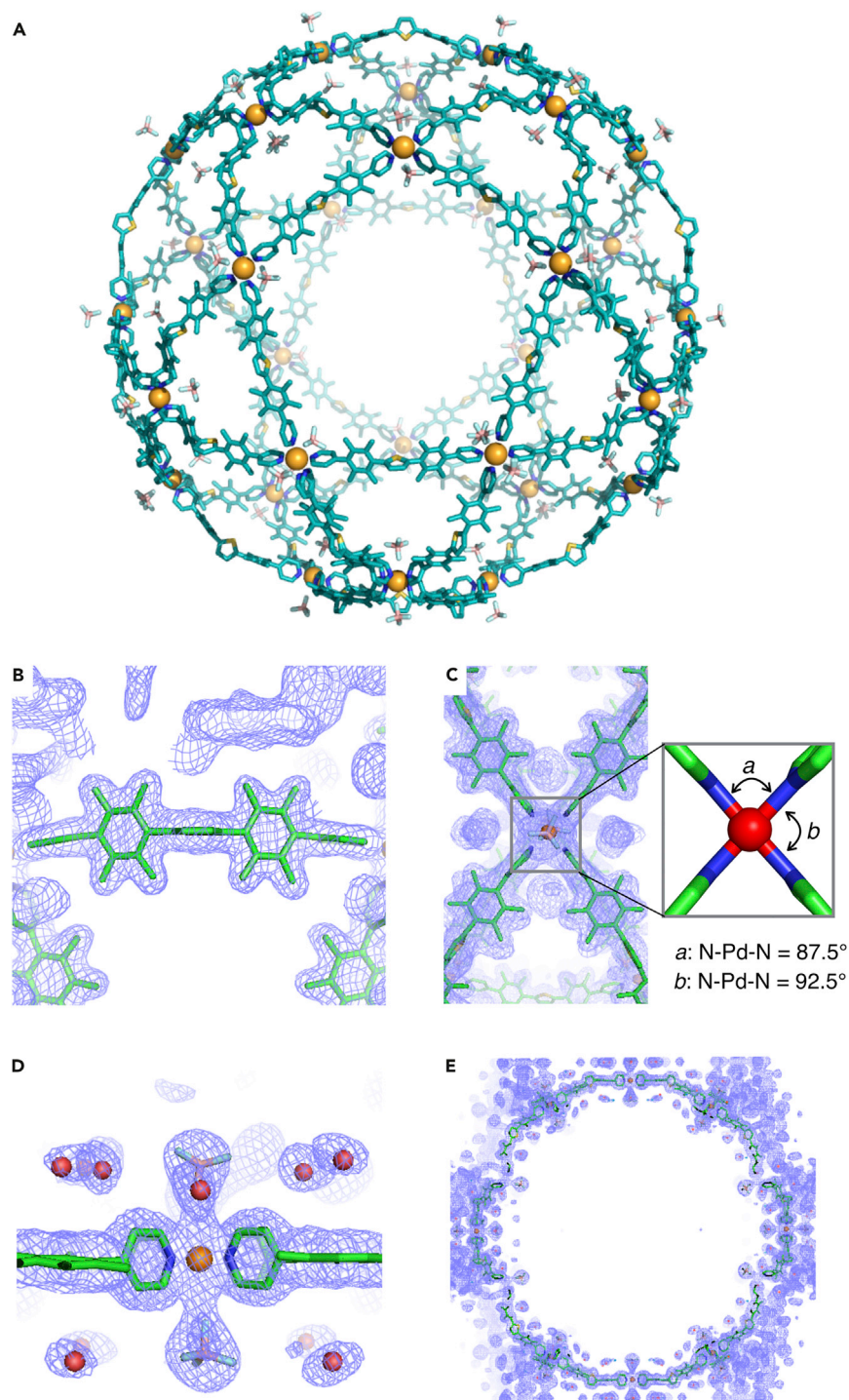


Figure 5. X-Ray Crystallographic Analysis of Complex 2d

Model building was carried out on the $2F_o - F_c$ and maximum entropy method electron-density map. Hydrogen atoms are not displayed for clarity.

(A) The entire view of the X-ray crystallographic structure of $M_{30}L_{60}$. A molecular structure with flawless icosidodecahedral symmetry was unveiled.

(B–D) An enlarged view around a ligand of $M_{30}L_{60}$. The modeled ligand structure clearly fits the observed electron density. (B) The ligand becomes slightly sagged upon sphere formation. (C) As a result, the N-Pd-N angles involved in the triangular and pentagon faces are adjusted to be close to

Figure 5. Continued

an ideal 90°. (D) Counter ions are ordered at the apical positions of the Pd(II) centers. Electron-density peaks attributed to DMSO molecules, which are coordinated to the ligands' aromatic rings (lone-pair- π interactions). Only oxygen atoms were modeled because of their severe disordering. (E) A sliced image of the complex with an electron-density map. No distinguishable electron-density peak was observed in the void space.

(90%), we perceive that the R factor (25.6%) and free R factor (27.0%) based on the observed structure factor F_o are quite reasonable.

Conclusions

In conclusion, we have succeeded in the self-assembly of an $M_{30}L_{60}$ spherical complex **4** and revealed its icosidodecahedral structure by X-ray crystallography. The exclusive formation of $M_{30}L_{60}$ was supported additionally by 1D ^1H NMR, ^1H DOSY NMR, and CSI-MS analysis. Considering the fact that ligands other than **3d** did not afford $M_{30}L_{60}$, even with the identical bend angle, fine-tuning of the flexibility was key for achieving the self-assembly of the $M_{30}L_{60}$ structure from a large number of components. The outer diameter of **4** reached more than 8 nm, and its interior space was as large as $157,000 \text{ \AA}^3$, undoubtedly one of the largest classes of well-defined synthetic molecules ever handled. The structure is highly promising as a scaffold for encapsulation of various nanomaterials such as metal nanoparticles⁴² or large proteins.^{39,43}

EXPERIMENTAL PROCEDURES**Synthesis of 3d**

A mixture of 2,5-bis(4,4,5,5-tetramethyl-1,3,2-dioxaborolan-2-yl)thiophene (101 mg, 0.30 mmol), 4-(4-iodo-2,3,5,6-tetramethylphenyl)pyridine (253 mg, 0.75 mmol), [1,1'-bis(diphenylphosphino)ferrocene]dichloropalladium complex with dichloromethane (31 mg, 0.038 mmol), and K_2CO_3 (414 mg, 3.0 mmol) in 1,2-dimethoxyethane (DME; 10 mL) and H_2O (1.0 mL) was stirred at 110°C for 14 hr under an Ar atmosphere. After cooling to the ambient temperature, the reaction mixture was filtered through a Celite pad, and the filtrate was evaporated in vacuo. The residue was purified by column chromatography on silica gel (ethyl acetate/hexane, 20:80 to 50:50) to give **3d** (85 mg, 57%) as a white solid.

Melting point: 279°C–281°C.

^1H NMR (500 MHz, CDCl_3 , 300 K): δ 8.68 (d, $J = 5.0$ Hz, 4H), 7.21 (d, $J = 5.0$ Hz, 4H), 6.92 (s, 2H), 2.13 (s, 12H), 1.88 (s, 12H). ^1H NMR (500 MHz, $\text{DMF-}d_7$, 300 K): δ 8.74 (d, $J = 6.0$ Hz, 4H), 7.27 (d, $J = 6.0$ Hz, 4H), 6.99 (s, 2H), 2.21 (s, 12H), 1.96 (s, 12H). Diffusion coefficient (500 MHz, $\text{DMF-}d_7$, 300 K): $\log D = -9.3$, $D = 5.01 \times 10^{-10} \text{ m}^2 \text{ s}^{-1}$.

^{13}C NMR (125 MHz, CDCl_3 , 300 K): δ 150.9 (C), 150.1 (CH), 143.0 (C), 139.6 (C), 134.6 (C), 134.0 (C), 131.1 (C), 126.6 (CH), 124.9 (CH), 18.1 (CH_3), 18.0 (CH_3).

IR: 2926, 1594, 1538, 1451, 1407, 1375, 1283, 1259, 1212, 1069, 1011, 979, 863, 804 cm^{-1} .

High-resolution mass spectrometry (electron-spray ionization time-of-flight): calculated for m/z $\text{C}_{34}\text{H}_{34}\text{N}_2\text{S} [\text{M} + \text{H}]^+$ 503.2531, found 503.2515.

Elemental analysis: calculated for $\text{C}_{34}\text{H}_{34}\text{N}_2\text{S}$ C, 81.23; H, 6.82; N, 5.57, found C, 80.94; H, 6.82; N, 5.57.

Self-Assembly of 4

To a solution of ligand **3d** (5.06 mg, 10 μmol) in $\text{DMF-}d_7$ (1.01 mL) was added a solution of $\text{Pd}(\text{BF}_4)_2(\text{CH}_3\text{CN})_4$ in $\text{DMF-}d_7$ (0.10 mL, 52.3 mM, 5.2 μmol), and the resulting mixture was stirred at 70°C for 12 hr. ^1H NMR spectroscopy confirmed the quantitative formation of the sphere complex **4**.

^1H NMR (500 MHz, $\text{DMF-}d_7$, 300 K): δ 9.75 (br, 240H), 7.75 (br, 240H), 6.98 (br, 120H), 2.13 (br, 720H), 1.89 (br, 360H), 1.69 (br, 360H); these two signals showed coalescence at 320 K. Diffusion coefficient (500 MHz, $\text{DMF-}d_7$, 300 K): $\log D = -10.3$, $D = 5.01 \times 10^{-11} \text{ m}^2 \text{ s}^{-1}$. ^{13}C NMR (150 MHz, $\text{DMF-}d_7$, 300 K): δ 156.4, 152.9, 143.7, 139.1, 135.5, 131.6, 129.6, 128.5, 18.5. The ^{13}C NMR spectrum was difficult to measure because of the severe broadness of the signals in $\text{DMF-}d_7$, and we finally obtained the spectrum after 232,000 acquisition attempts on a 600 MHz NMR system equipped with a gradient cold probe (53040HCNVC).

Crystallographic Analysis of 4

Colorless crystals of $\text{M}_{30}\text{L}_{60}$ were obtained by vapor diffusion of isopropyl acetate into a DMSO solution of **4** (with tetrafluoroborate as the counter anion). The preliminary diffraction studies were performed at the BL41XU beamline at SPring-8 (Rayonix MX225H&E CCD detector) and the BL1A beamline at KEK PF-AR (Dectris PILATUS 2M-F PAD detector) at 296 K. The final diffraction data were measured at the BL38B1 beamline at SPring-8 (Rayonix MX225H&E CCD detector). HKL2000⁴⁴ was used for the processing and data reduction in the $C2$ space group. The structure was solved and refined by SHELX⁴⁰ in the $C2/m$ space group. These data did not have a high enough resolution for calculation of the hydrogen positions. The crystal lattice contained huge voids (90.0%) with a lot of disordered solvents and anions. Because of the very moderate diffraction power of the crystal (resolution 2.0 Å), solvent molecules could not be located as realistic molecular structures, and instead, oxygen atoms (DMSO) were located for the residual electron density with full or partial occupancies until a plateau of ca. 0.6 $\text{e}/\text{\AA}^3$ was reached in the maximum entropy density map. The ligands showed very large thermal motion (maybe as a result of positional disorder, which however, could not be modeled), and thus a multitude of bond distance and thermal parameter restraints (DFIX, DANG, and FLAT) to the ligands, counter anions, and Pd-N distances had to be applied in order to avoid chemically unreasonable bond distances and angles. Pd atoms were refined anisotropically, and all other atoms were refined isotropically.

ACCESSION NUMBERS

The $\text{M}_{30}\text{L}_{60}$ structure reported in this article has been deposited in the Cambridge Crystallographic Data Centre under accession number CCDC: 1482268.

SUPPLEMENTAL INFORMATION

Supplemental Information includes Supplemental Experimental Procedures, 26 figures, one table, and one crystallographic data file and can be found with this article online at <http://dx.doi.org/10.1016/j.chempr.2016.06.007>.

AUTHOR CONTRIBUTIONS

Conceptualization, M.F.; Methodology, D.F. and Y.U.; Investigation, D.F., Y.U., S.S., and H.Y.; Formal Analysis, D.F., S.S., N.M., and T.K.; Writing – Original Draft, D.F. and Y.U.; Review & Editing, D.F. and M.F.; Funding Acquisition, D.F. and M.F.; Supervision, M.F.

ACKNOWLEDGMENTS

This work was supported by the JST-ACCEL program and the PRESTO program, partly supported by KAKENHI (25102007). The synchrotron X-ray crystallography was performed at the BL1A beamline at the KEK Photon Factory (2015G097) and at the BL38B1 and BL41XU beamlines at SPring-8 (2014A0042 and 2015B0120).

Received: April 27, 2016

Revised: June 1, 2016

Accepted: June 9, 2016

Published: July 7, 2016

REFERENCES AND NOTES

1. Lawson, D.M., Artymiuk, P.J., Yewdall, S.J., Smith, J.M., Livingstone, J.C., Treffry, A., Luzzago, A., Levi, S., Arosio, P., and Cesareni, G. (1991). Solving the structure of human H ferritin by genetically engineering intermolecular crystal contacts. *Nature* 349, 541–544.
2. Stagg, S.M., Gürkan, C., Fowler, D.M., LaPointe, P., Foss, T.R., Potter, C.S., Carragher, B., and Balch, W.E. (2006). Structure of the Sec13/31 COPII coat cage. *Nature* 439, 234–238.
3. Stagg, S.M., LaPointe, P., Razvi, A., Gürkan, C., Potter, C.S., Carragher, B., and Balch, W.E. (2008). Structural basis for cargo regulation of COPII coat assembly. *Cell* 134, 474–484.
4. Grimes, J.M., Burroughs, J.N., Gouet, P., Diprose, J.M., Malby, R., Zióntara, S., Mertens, P.P., and Stuart, D.I. (1998). The atomic structure of the bluetongue virus core. *Nature* 395, 470–478.
5. Zhang, X., Boyce, M., Bhattacharya, B., Zhang, X., Schein, S., Roy, P., and Zhou, Z.H. (2010). Bluetongue virus coat protein VP2 contains sialic acid-binding domains, and VP5 resembles enveloped virus fusion proteins. *Proc. Natl. Acad. Sci. USA* 107, 6292–6297.
6. Steed, J., and Gale, P., eds. (2012). *Supramolecular Chemistry: From Molecules to Nanomaterials* (John Wiley).
7. Conn, M.M., and Rebek, J. (1997). Self-assembling capsules. *Chem. Rev.* 97, 1647–1668.
8. Caulder, D.L., and Raymond, K.N. (1999). Supermolecules by design. *Acc. Chem. Res.* 32, 975–982.
9. Fujita, M., Tominaga, M., Hori, A., and Therrien, B. (2005). Coordination assemblies from a Pd(II)-cornered square complex. *Acc. Chem. Res.* 38, 369–378.
10. Saalfrank, R.W., Maid, H., and Scheurer, A. (2008). Supramolecular coordination chemistry: the synergistic effect of serendipity and rational design. *Angew. Chem. Int. Ed. Engl.* 47, 8794–8824.
11. Forgan, R.S., Sauvage, J.-P., and Stoddart, J.F. (2011). Chemical topology: complex molecular knots, links, and entanglements. *Chem. Rev.* 111, 5434–5464.
12. Chakrabarty, R., Mukherjee, P.S., and Stang, P.J. (2011). Supramolecular coordination: self-assembly of finite two- and three-dimensional ensembles. *Chem. Rev.* 111, 6810–6918.
13. Young, N.J., and Hay, B.P. (2013). Structural design principles for self-assembled coordination polygons and polyhedra. *Chem. Commun.* 49, 1354.
14. Smulders, M.M.J., Riddell, I.A., Browne, C., and Nitschke, J.R. (2013). Building on architectural principles for three-dimensional metallosupramolecular construction. *Chem. Soc. Rev.* 42, 1728–1754.
15. Saalfrank, R.W., Stark, A., Peters, K., and Schnering von, H.G. (1988). The first “adamantoid” alkaline earth metal chelate complex: synthesis, structure, and reactivity. *Angew. Chem. Int. Ed. Engl.* 27, 851–853.
16. Fujita, M., Oguro, D., Miyazawa, M., Oka, H., Yamaguchi, K., and Ogura, K. (1995). Self-assembly of ten molecules into nanometre-sized organic host frameworks. *Nature* 378, 469–471.
17. MacGillivray, L.R., and Atwood, J.L. (1997). A chiral spherical molecular assembly held together by 60 hydrogen bonds. *Nature* 389, 469–472.
18. Stang, P.J., Olenyuk, B., Muddiman, D.C., and Smith, R.D. (1997). Transition-metal-mediated rational design and self-assembly of chiral, nanoscale supramolecular polyhedra with unique T symmetry. *Organometallics* 16, 3094–3096.
19. Caulder, D.L., Powers, R.E., Parac, T.N., and Raymond, K.N. (1998). The self-assembly of a pre-designed tetrahedral M4L6 supramolecular cluster. *Angew. Chem. Int. Ed. Engl.* 37, 1840–1843.
20. Abrahams, B.F., Egan, S.J., and Robson, R. (1999). A very large metallosupramolecular capsule with cube-like 43 topology assembled from twelve Cu(II) centers and eight tri-bidentate tri-anionic ligands derived from 2,4,6-triphenylazo-1,3,5-trihydroxybenzene. *J. Am. Chem. Soc.* 121, 3535–3536.
21. Takeda, N., Umemoto, K., Yamaguchi, K., and Fujita, M. (1999). A nanometre-sized hexahedral coordination capsule assembled from 24 components. *Nature* 398, 794–796.
22. Olenyuk, B., Whiteford, J.A., Fechtenkötter, A., and Stang, P.J. (1999). Self-assembly of nanoscale cuboctahedra by coordination chemistry. *Nature* 398, 796–799.
23. Moulton, B., Lu, J., Mondal, A., and Zaworotko, M.J. (2001). Nanoballs: nanoscale faceted polyhedra with large windows and cavities. *Chem. Commun.* 863–864.
24. Eddaoudi, M., Kim, J., Wachter, J.B., Chae, H.K., O’Keeffe, M., and Yaghi, O.M. (2001). Porous metal-organic polyhedra: 25 Å cuboctahedron constructed from 12 Cu₂(CO₂)₄ paddle-wheel building blocks. *J. Am. Chem. Soc.* 123, 4368–4369.
25. Li, J.-R., and Zhou, H.-C. (2010). Bridging-ligand-substitution strategy for the preparation of metal-organic polyhedra. *Nat. Chem.* 2, 893–898.
26. Pasquale, S., Sattin, S., Escudero-Adán, E.C., Martínez-Belmonte, M., and de Mendoza, J. (2012). Giant regular polyhedra from calixarene carboxylates and uranyl. *Nat. Commun.* 3, 785.
27. Bilbeisi, R.A., Ronson, T.K., and Nitschke, J.R. (2013). A self-assembled [FeII₁₂L₁₂] capsule with an icosahedral framework. *Angew. Chem. Int. Ed. Engl.* 52, 9027–9030.
28. Harris, K., Fujita, D., and Fujita, M. (2013). Giant hollow MnL_{2n} spherical complexes: structure, functionalisation and applications. *Chem. Commun.* 49, 6703.
29. Suzuki, K., Tominaga, M., Kawano, M., and Fujita, M. (2009b). Self-assembly of an M₆L₁₂ coordination cube. *Chem. Commun.* 1638–1643.
30. Tominaga, M., Suzuki, K., Kawano, M., Kusakawa, T., Ozeki, T., Sakamoto, S., Yamaguchi, K., and Fujita, M. (2004). Finite, spherical coordination networks that self-organize from 36 small components. *Angew. Chem. Int. Ed. Engl.* 43, 5621–5625.
31. Sun, Q.F., Iwasa, J., Ogawa, D., Ishido, Y., Sato, S., Ozeki, T., Sei, Y., Yamaguchi, K., and Fujita, M. (2010). Self-assembled M₂₄L₄₈ polyhedra and their sharp structural switch upon subtle ligand variation. *Science* 328, 1144–1147.
32. Pain, R.H., ed. (1994). *Mechanisms of Protein Folding* (IRL Press).
33. Fujita, D., Yokoyama, H., Ueda, Y., Sato, S., and Fujita, M. (2015). Geometrically restricted intermediates in the self-assembly of an M₁₂L₂₄ cuboctahedral complex. *Angew. Chem. Int. Ed. Engl.* 54, 155–158.

34. Yokoyama, H., Ueda, Y., Fujita, D., Sato, S., and Fujita, M. (2015). Finely resolved threshold for the sharp M12L24/M24L48 structural switch in multi-component MnL2n polyhedral assemblies: X-ray, MS, NMR, and ultracentrifugation analyses. *Chem. Asian J.* **10**, 2292–2295.
35. Sato, S., Iida, J., Suzuki, K., Kawano, M., Ozeki, T., and Fujita, M. (2006). Fluorous nanodroplets structurally confined in an organopalladium sphere. *Science* **313**, 1273–1276.
36. Fujita, D., Takahashi, A., Sato, S., and Fujita, M. (2011). Self-assembly of Pt(II) spherical complexes via temporary labilization of the metal-ligand association in 2,2,2-trifluoroethanol. *J. Am. Chem. Soc.* **133**, 13317–13319.
37. Yamaguchi, K. (2003). Cold-spray ionization mass spectrometry: principle and applications. *J. Mass Spectrom.* **38**, 473–490.
38. Takata, M. (2008). The MEM/Rietveld method with nano-applications – accurate charge-density studies of nano-structured materials by synchrotron-radiation powder diffraction. *Acta Crystallogr. A* **64**, 232–245.
39. Fujita, D., Suzuki, K., Sato, S., Yagi-Utsumi, M., Yamaguchi, Y., Mizuno, N., Kumasaka, T., Takata, M., Noda, M., Uchiyama, S., et al. (2012). Protein encapsulation within synthetic molecular hosts. *Nat. Commun.* **3**, 1093–1097.
40. Sheldrick, G.M. (2015). Crystal structure refinement with SHELXL. *Acta Crystallogr. C Struct. Chem.* **71**, 3–8.
41. Zukerman-Schpector, J., and Tiekink, E.R.T. (2014). On the role of DMSO-O(lone pair)⋯π(arene), DMSO-S(lone pair)⋯π(arene) and SO⋯π(arene) interactions in the crystal structures of dimethyl sulphoxide (DMSO) solvates. *CrystEngComm* **16**, 6398–6407.
42. Suzuki, K., Sato, S., and Fujita, M. (2009). Template synthesis of precisely monodisperse silica nanoparticles within self-assembled organometallic spheres. *Nat. Chem.* **2**, 25–29.
43. Fujita, D. (2014). Challenges to large molecular encapsulation. *Pure Appl. Chem.* **1**, 3–11.
44. Otwinowski, Z., and Minor, W. (1997). Processing of X-ray diffraction data collected in oscillation mode. *Methods Enzymol.* **276**, 307–326.